Available online at www.sciencedirect.com
ScienceDirect
Catalysis Today 130 (2008) 382–388
CATALYSIS TODAY
www.elsevier.com/locate/cattod

Preparing and characterizing the active carbon produced by steam and carbon dioxide as a heavy oil hydrocracking catalyst support

Hidetsugu Fukuyama *, Satoshi Terai

Technology Research Center, Toyo Engineering Corporation, 6-3 Akanehama 2-chome, Narashino-shi, Chiba 275-0024, Japan

Available online 26 November 2007

Abstract

Active carbon was prepared from Yallourn brown coal char using steam and carbon dioxide activation in a laboratory rotary kiln. The activation rate with steam was faster than that with carbon dioxide. The pore structure of the active carbons was characterized using the nitrogen isotherms at 77 K. The pore volume and specific surface area of the active carbon increased with the carbon burn-off, and compared to carbon dioxide, steam activation produced active carbon that was richer in mesopores by increasing the pore size from micropores to mesopores. The porosity of the active carbons was related to the ability to adsorb maltene, the normal hexane-soluble fraction, in the vacuum residue of petroleum crude. The steam-activated carbon rich in mesopores had a greater ability to adsorb maltene, which consists of large-molecular-weight hydrocarbons.

Keywords: Active carbon; Catalyst support; Nitrogen isotherms; Porosity; Maltene

1. Introduction

Heavy crude contains impurities such as asphaltenes, sulfur, nitrogen, and heavy metals (nickel and vanadium), which are more concentrated in the higher boiling point fraction of crude oil. The coking that results from the polycondensation of high-molecular-weight asphaltenes and the deposition of heavy metals deactivates the catalyst used for hydrocracking heavy oil. The conventionally used acid sites on alumina contribute to its high cracking activity, although they are deactivated by N-containing compounds or the coke formed by the poly-condensation of heavy hydrocarbon compounds on the surface [1,2]. Carbon is neutral or a weak base in nature, and recent studies have examined its use as a catalyst for heavy oil hydrocracking because of its high surface area, variable pore size, surface functional groups, and ability to take up heavy metals and resist coke deposition. López-Salinas et al. [3] studied alumina–carbon black composite supports with a view to diminish either strength and/or number of acid sites.

Rodríguez-Reinoso [4] reviewed the use of carbon materials as catalysts or for catalyst support, and reported that mesopores and macropores play important roles in adsorption, serving as passages for the adsorbate. Lillian [5] described its potential advantages in residue processing over carbon-supported catalysts, and Derbyshire et al. [6] showed that the pore structure of carbon has advantages in reactions involving large molecules, such as the hydrogenation of liquids with high boiling points. Molina-Sabio et al. [7] studied the effect of steam and carbon dioxide activation on the distribution of micropores in activated carbon made from olive stone char and found that steam resulted in a greater volume of meso- and macropores than activated carbon prepared using carbon dioxide.

In this study, active carbons were prepared from Australian Yallourn brown coal char (YC) using steam and carbon dioxide activation in a laboratory rotary kiln; they were to be applied as a catalyst support with larger pores for the hydrocracking of heavy oil. The porosity of the prepared active carbons was characterized using nitrogen isotherms and examined in relation to carbon burn-off. The steam-activated carbons were rich in mesopores, which have a high ability to adsorb maltene, the normal hexane-soluble fraction, from vacuum residue.

2. Experimental

2.1. Preparation of active carbon

YC with the properties shown in Table 1 was used as the raw material. Approximately, 190 g of pulverized YC consisting of

* Corresponding author. Tel.: +81 47 408 2371; fax: +81 45 408 2372.
E-mail address: fukuyama@ga.toyo-eng.co.jp (H. Fukuyama).

0920-5861/$ – see front matter
doi:10.1016/j.cattod.2007.10.034

Table 1
Properties of Yallourn brown coal char

Moisture	Volatiles	Fixed carbon	Ash
Proximate analysis (wt%)			
10.5	9.7	87.4	2.9

C	H	N	S	O (balance)
Ultimate analysis (wt% d.a.f[a])				
91.3	1.3	1.0	0.2	6.1

[a] Dry ash-free.

particles from 355 to 840 μm in size were loaded into the 1-L retort of a laboratory rotary kiln. The YC sample was heated to 473 K under nitrogen flow for drying for 1 h while the retort rotated at 6 rpm. The sample was heated at 50 K/h to the target activation temperature, then, the activation gas, steam or carbon dioxide, was introduced. The activation temperature (973–1123 K) and time (6–180 min) were varied to obtain active carbons with different burn-offs. After activation, the sample was cooled under a nitrogen flow and removed from the retort at ambient temperature. The diagram of preparation of active carbon is shown in Fig. 1.

2.2. Characterization of pore texture

The nitrogen isotherm of the active carbon was obtained at 77 K using a NOVA-1000 (Quantachrome Instruments, Boynton Beach, FL, USA) to characterize the porosity of the active carbon. The Brunauer–Emmett–Teller (BET)-specific surface area (S_{BET}) of the active carbon was calculated from the isotherms using the linear form of the BET equation. The pore volume distribution was obtained with the Barrett–Joyner–Halenda (BJH) method using the cylindrical pore model. The pore volume (V_{micro}) and the specific surface area (S_{micro}) of micropores ($d < 2$ nm) were calculated using the *t*-plot method. The specific surface area (S_{meso}) of mesopores ($d \geq 2$ nm) was obtained by subtracting S_{micro} from S_{BET}. The pore volume of mesopore (V_{meso}) was obtained subtracting

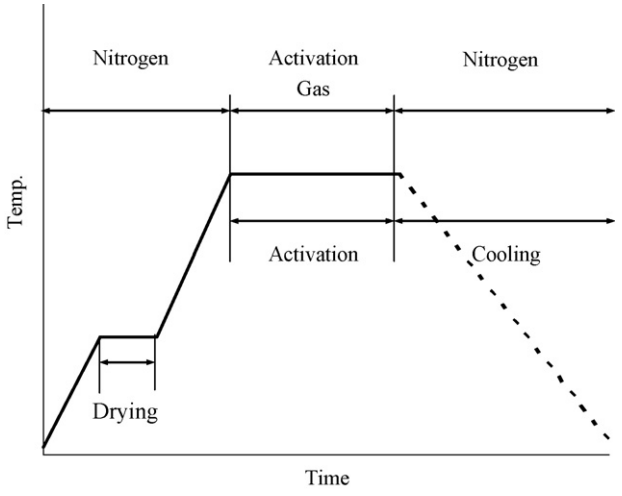

Fig. 1. Diagram of preparation of active carbon.

Table 2
Properties of the vacuum residue of petroleum crude

Gravity API	5.3
Total sulfur, wt%	4.02
Nitrogen, wt%	0.53
CCR, wt%	22.4
Metal Ni/V, wppm	53/180
C/H, wt%	84.8/10.2

V_{micro} from the total pore volume (V_{total}) which was calculated from the adsorbed nitrogen amount at relative pressure 0.98.

2.3. Maltene adsorption

The ability of the active carbon to adsorb maltene was studied in relation to the pore structure of the active carbons.

Some authors, Yamazoe [8] and Kotlyar et al. [9], reported the use of absorbance to measure the content of maltene or asphaltene in oil. In this study a maltene containing solution was prepared by dissolving vacuum residue (0.2571 g) in 1000 mL of normal hexane at room temperature. The properties of the vacuum residue are shown in Table 2. The solution was filtered through JIS No. 5A filter paper (equivalent to Whatman No. 412) and the filtrate was used as the maltene containing solution. Since the maltene containing solution is brown, the absorbance of different maltene concentrations prepared by dilution with normal hexane at 600 nm had previously been calibrated.

Precisely weighed active carbon (1.88 g) was immersed in 25 mL of maltene solution. The change in the maltene concentration with immersion time was monitored by measuring the absorbance of the supernatant using the calibration curve and compared to the initial maltene concentration.

The maltene adsorption ability of carbon samples activated using steam and a commercial reference active carbon 4GSS (Tsurumicoal, Yokohama, Japan) were used for the evaluation.

3. Results

3.1. Preparation of activated carbon

The conditions used for activation and the burn-off of raw materials are listed in Table 3. The term burn-off is defined as the mass of carbon reacted relative to the mass of fixed carbon (FC) in the YC sample before activation, and is calculated using the equation:

$$\text{Burn-off}\ (\%) = \left(1 - \left(\frac{\text{the weight of sample after activation}}{\text{the weight of FC in the sample before activation}}\right)\right) \times 100.$$

The burn-off is plotted against the activation time using steam and carbon dioxide in Fig. 2. The burn-off increased with activation time. Higher activation temperature increased the gasification rate. Higher flow rate (mol/min/100 g-FC) of activation gas increased the gasification rate. The gasification

Table 3
Activation condition and burn-off

Sample no.	Activation gas	Flow rate (mol/min/100 g-FC[a])	Temperature (K)	Time (h)	Burn-off (%)
1	CO_2	0.082	1123	0.1	7.8
2	CO_2	0.082	1123	0.3	11.8
3	CO_2	0.082	1123	2.5	50.1
4	CO_2	0.082	1123	3.0	59.9
5	CO_2	0.201	1123	0.4	21.6
6	CO_2	0.201	1123	1.0	30.3
7	CO_2	0.082	1073	0.5	8.9
8	CO_2	0.082	1073	1.0	14.0
9	H_2O	0.213	973	1.7	19.8
10	H_2O	0.055	1073	2.0	36.6
11	H_2O	0.120	1073	0.1	8.0
12	H_2O	0.120	1073	0.1	8.7
13	H_2O	0.213	1073	0.4	24.8
14	H_2O	0.120	1073	0.7	30.7
15	H_2O	0.120	1073	0.7	25.0
16	H_2O	0.120	1073	0.7	25.9
17	H_2O	0.120	1073	1.3	40.6
18	H_2O	0.120	1073	2.0	55.0
19	H_2O	0.120	1073	2.0	57.1
20	H_2O	0.120	1073	2.7	67.2
21	H_2O	0.416	1073	1.0	55.4
22	H_2O	0.065	1123	1.0	30.8
23	H_2O	0.213	1123	0.4	39.1
24	H_2O	0.213	1123	1.0	62.9
25	H_2O	0.416	1123	0.5	51.5
26	H_2O	0.213	1173	0.4	49.9

[a] Fixed carbon.

rate of carbon dioxide at 1123 K even with higher flow rate (0.201 mol/min/100 g-FC) than steam (0.120 mol/min/100 g-FC) was similar to that of steam at 1073 K.

3.2. Characterization of pore texture

The adsorption and desorption isotherms of carbon dioxide- and steam-activated carbons with different burn-offs are shown in Figs. 3 and 4, respectively.

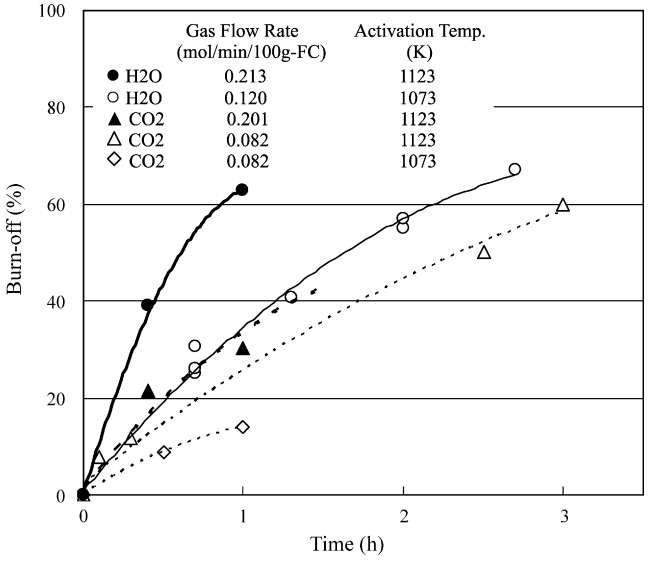

Fig. 2. Plot of activation time vs. burn-off.

A shift in the isotherm type, which was classified using the method of Sing et al. [10], was observed from I to II with the increase in burn-off, reflecting the development of mesopores. This was observed more for steam-activated carbons.

When the adsorption isotherms of steam-activated carbon at 57.1% burn-off in Fig. 4 and carbon dioxide-activated carbon at

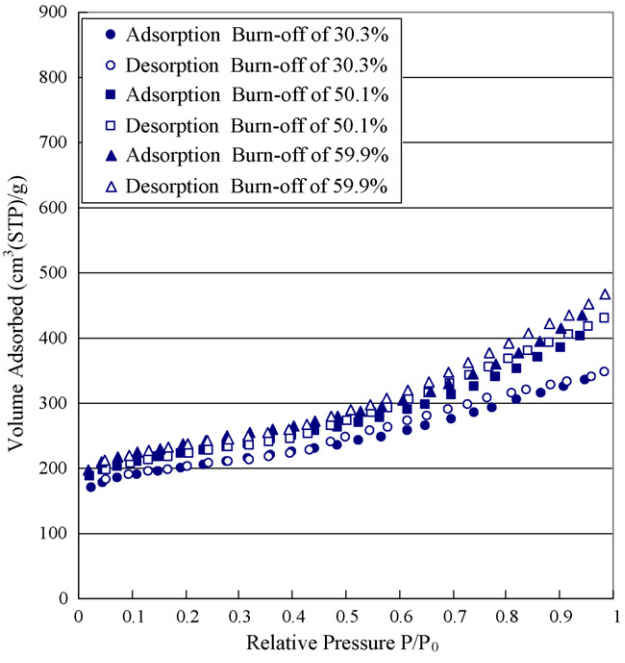

Fig. 3. Nitrogen isotherms of carbon dioxide-activated carbons.

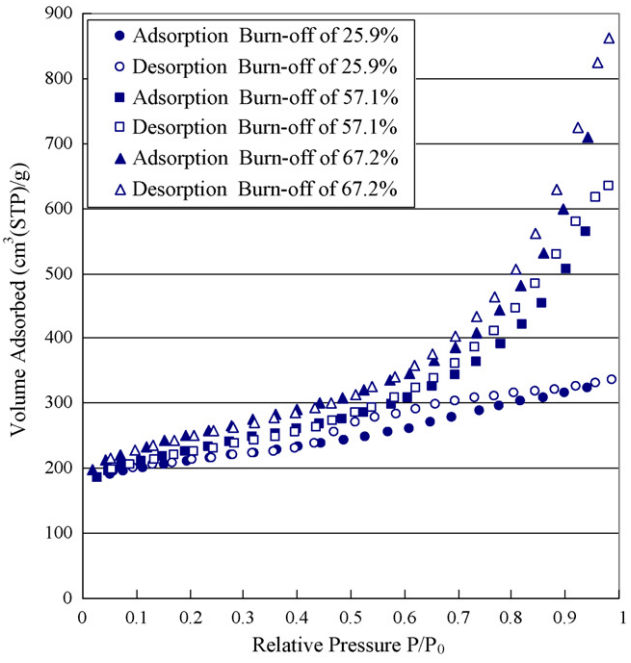

Fig. 4. Nitrogen isotherms of steam-activated carbons.

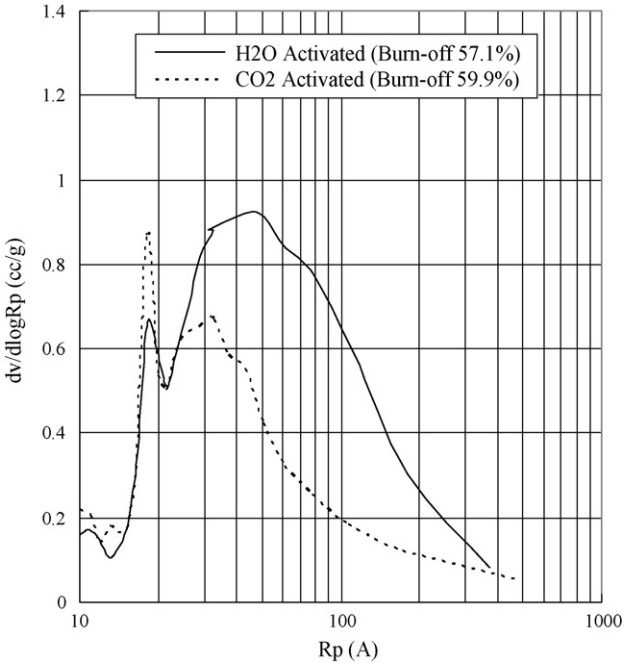

Fig. 5. Pore size distribution of steam- and carbon dioxide-activated carbons.

59.9% burn-off in Fig. 3 are compared, both isotherms were similar up to relative pressures of 0.5. At higher relative pressures, the steam-activated carbon adsorbed more nitrogen than the carbon dioxide-activated carbon, which had a greater burn-off than the steam-activated carbon. The isotherm of the steam-activated carbon suggests that it was more porous. As shown in Fig. 5, the steam-activated carbon had a greater pore distribution than the carbon dioxide-activated carbon.

Table 4
Pore data of active carbons

Sample no.	Specific surface area (m^2/g)			Pore volume (cm^3/g)		
	S_{BET}	S_{micro}	S_{meso}	V_{total}	V_{micro}	V_{meso}
1	–	–	–	–	–	–
2	640	–	–	0.280	–	–
3	818	503	315	0.660	0.210	0.450
4	884	545	339	0.721	0.220	0.501
5	628	500	128	0.378	0.223	0.155
6	739	497	242	0.530	0.210	0.320
7	523	495	28	0.255	0.214	0.041
8	590	545	45	0.298	0.239	0.059
9	589	474	115	0.354	0.207	0.147
10	748	457	291	0.578	0.180	0.398
11	550	518	32	0.280	0.230	0.050
12	556	524	32	0.271	0.220	0.051
13	657	485	172	0.418	0.203	0.215
14	920	–	–	0.520	–	–
15	681	495	186	0.460	0.220	0.240
16	795	582	213	0.518	0.240	0.278
17	773	419	354	0.660	0.150	0.510
18	878	341	537	1.040	0.110	0.930
19	825	312	513	0.980	0.095	0.885
20	914	295	619	1.331	0.074	1.257
21	846	328	518	0.971	0.110	0.861
22	–	–	–	–	–	–
23	980	–	–	0.610	–	–
24	937	368	569	1.140	0.115	1.025
25	–	–	–	–	–	–
26	–	–	–	–	–	–
4GSS[a]	1300	1281	19	0.568	0.527	0.041

[a] Commercial active carbon used as a reference for maltene adsorption test.

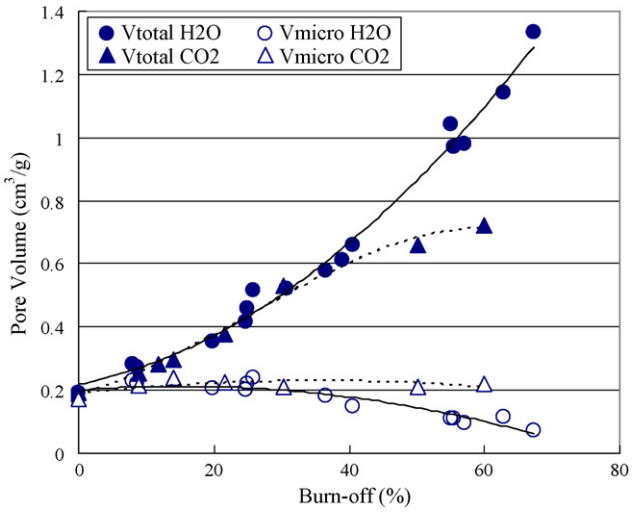

Fig. 6. Evolution of pore volume as a function of burn-off.

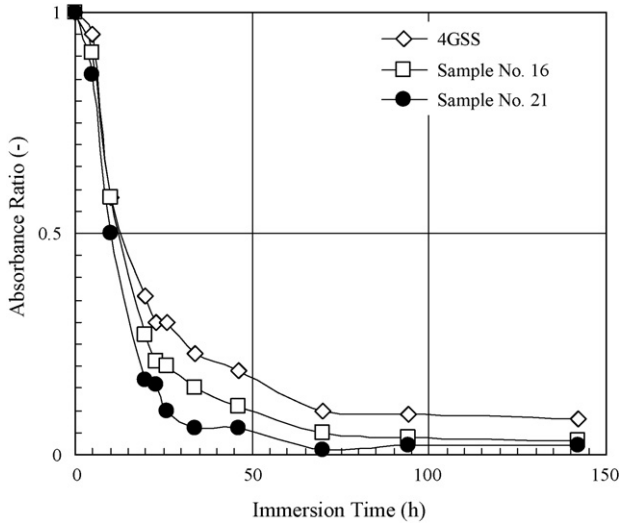

Fig. 8. Change in the absorbance with immersion time.

Pore texture data for the obtained active carbons are listed in Table 4. The evolution of pore volume as a function of burn-off for steam- and carbon dioxide-activated carbon is illustrated in Fig. 6. With steam and carbon dioxide, the total pore volume increased with the burn-off and the micropore volume was constant up to a burn-off of about 30%. Above a burn-off of about 30%, the total pore volume of the carbon dioxide-activated carbon increased via mesopore evolution only. For the steam-activated carbon, the total pore volume increased more steeply than for the carbon dioxide-activated carbon, while the micropores decreased.

The relationships between burn-off and the specific surface areas of the steam- and carbon dioxide-activated carbons are illustrated in Fig. 7. The micropore-specific surface area of steam-activated carbon decreased above a burn-off of about 30%, while that of carbon dioxide-activated carbon remained almost constant. The increase in the total specific surface area with steam lies on the same line as that for carbon dioxide-activated carbon. The increase in the total specific surface area with steam was not as steep as the increase in the total pore volume, as shown in Fig. 6.

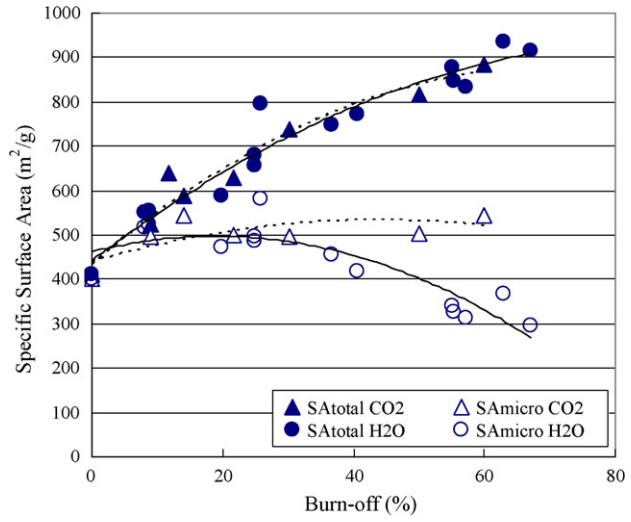

Fig. 7. Evolution of specific surface area as a function of burn-off.

3.3. Maltene adsorption

The active carbons, No. 16, No. 21 and 4GSS of which pore data are listed in Table 4, were used for the immersion test as typical active carbon with different pore texture.

The absorbance of the supernatant, which is related to the maltene concentration, decreased with the immersion time, as shown in Fig. 8. Initially, the absorbance decreased rapidly for all of the active carbon samples, and then the decrease gradually approached a limit that depended on the respective active carbon adsorption capacity.

Active carbon No. 21, which was the richest in mesopores, had the highest maltene adsorption, while the micropore-rich active carbon 4GSS had the lowest adsorption.

4. Discussion

4.1. Preparation of active carbon

Since both gasification reactions of carbon with steam and with carbon dioxide are endothermic, the higher activation temperature enhances the gasification as shown in Fig. 2. The activation by steam was faster than by carbon dioxide, which concurs with other studies [11–13]. The mechanisms of gasification reaction are discussed by Wigmans [14] that the rate of dissociation and adsorption of intermediate of steam (*i.e.*, H_2O) to gasifiable active site C^*, ($C^* + H_2O \leftrightarrow C(O) + H_2$), is faster than that of CO_2, ($C^* + CO_2 \leftrightarrow C(O) + CO$). For further difference between the reaction with steam and with carbon dioxide, Wigmans [14] explained that the larger carbon dioxide molecule compared to steam restricts the ability of carbon dioxide to diffuse through the pores in the carbon and to access the gasifiable sites of inner pore, which results in slower gasification by carbon dioxide than by steam.

4.2. Characterization of pore texture

The increase in the porosity of active carbon activated with either steam or carbon dioxide was similar up to 30% burn-off, as shown in Fig. 6. It is conceivable that this initial increase in pore volume resulted from the readily gasifiable material at the carbon surface causing mesopores to evolve. At above about 30% burn-off, the total pore volume of the carbon dioxide-activated carbon increased from the evolution of mesopores, while the micropore volume remained constant. In contrast, the total pore volume of the steam-activated carbon increased more rapidly, resulting from mesopore evolution, which was mainly attributable to the enlargement of micropores into mesopores. The increase in the total specific surface area with steam was not as steep as the increase in the total pore volume, as shown in Fig. 6, deduced from the reduced contribution of mesopores to the increase in the specific surface area compared to that of micropores.

Pastor-Villegas and Durán-Valle [15] reported that steam produces much more mesoporosity than carbon dioxide, especially at activation temperatures of 973–1123 K. As Rodríguez-Reinoso et al. [13] discussed, it is likely that gasification occurs only from the surface of carbon material with carbon dioxide, which is larger than a water molecule, and the number of sites accessible by carbon dioxide decreases gradually as the burn-off increases. In contrast, the smaller steam molecule can access existing micropores and enlarge them. Therefore, steam favored mesopore formation by enlarging micropores as the burn-off progressed.

Molina-Sabio et al. [7] further studied the pore structure of active carbon in relation to the amount of oxygen functional groups. They found that the larger amount of oxygen functional groups, the higher micropore volume and the only slight increase of oxygen functional groups with the increase of burn-off of steam-activated carbon and reported that the activation by steam is producing a change from micro- to meso- and macropores by removal of carbon atoms mainly from the entrance of the micropores.

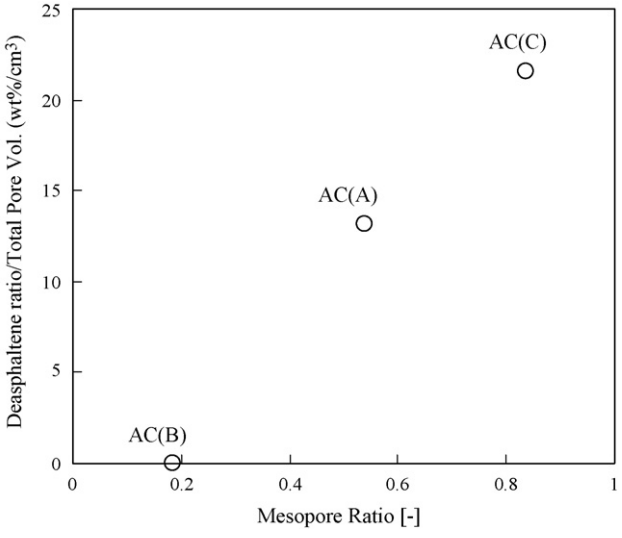

Fig. 9. Relationship between deasphalting and the mesopores in active carbon [17].

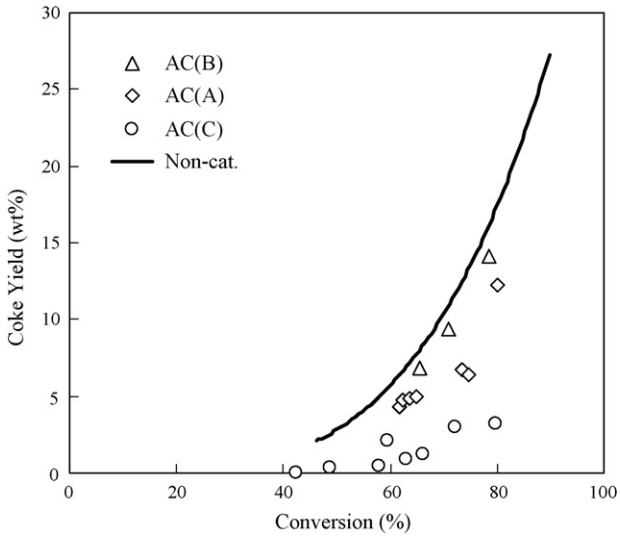

Fig. 10. Effect of AC pore structure on the coke yield during hydrocracking at 7 MPa [17] mesopore ratio: AC(C) > AC(A) > AC(B).

4.3. Maltene adsorption

The active carbon 4GSS had a greater pore volume than active carbon No. 16, but the highest surface area resulted from having the smallest pores, as shown in Table 4. Active carbon No. 21 had the most mesopores. Assuming the cylindrical pore model, the average pore diameters of respective active carbon are calculated as 1.74 nm for 4GSS, 2.60 nm for No. 16 and 4.56 nm for No. 21. Hall and Herron [16] studied the molecular sizes of asphaltene and maltene in petroleum residue using gel permeation chromatography (GPC) and reported that the mean size of asphaltene is 7.5–6 nm and that of maltene is 3–4 nm. Since active carbon No. 21 has an average pore diameter of 4.56 nm, it will be able to accommodate relatively large maltene molecules.

Following the pre-evaluation by this maltene adsorption test, elsewhere [17], we further carried out the asphaltene adsorption test under hydrogen pressure 10 MPa at 523 K and found that the mesopore-rich active carbon shows higher deasphaltene ratio meaning more adsorption ability of asphaltenes in vacuum residue as shown in Fig. 9. We also carried out the hydrocracking test of vacuum residue using active carbons with different pore textures as catalyst supports and found that the mesopore-rich active carbon support is effective at preventing coke formation during the hydrocracking of vacuum residue, which involves large hydrocarbon molecules, as shown in Fig. 10.

5. Conclusions

Various active carbons were prepared from YC using steam and carbon dioxide activation in a laboratory rotary kiln. The activation rate with steam was faster than with carbon dioxide.

The porosity of the active carbons characterized using the nitrogen isotherms at 77 K was a function of the burn-off. The increase in the total pore volume of carbon dioxide-activated carbon was attributed to mesopore evolution. Above about 30%

burn-off, the total pore volume of steam-activated carbon increased mainly via the evolution of mesopores, which were produced from the enlargement of micropores.

The porosity of the active carbons was related to their ability to adsorb maltene, the normal hexane-soluble fraction, in the vacuum residue of petroleum crude. The steam-activated carbon rich in mesopores had a greater ability to adsorb maltene, which consists of large hydrocarbon molecules. Therefore, steam activation favors the formation of active carbon with mesopores, which are suitable for hydrocracking heavy oil.

Acknowledgment

The fundamental work was conducted as a research project of the Petroleum Energy Center with a subsidy from the former Ministry of International Trade and Industry, Japan.

References

[1] M. Absi-Halabi, A. Stanislaus, D.L. Trimm, Appl. Catal. 72 (1991) 193–215.
[2] M.R. Gray, F. Khorasheh, S.E. Wanke, U. Achida, A. Krzywicki, E.C. Sanford, O.K.Y. Sy, M. Ternan, Energy Fuels 6 (1992) 478–485.
[3] E. López, J.G. Espinosa, J.G. Hernández-Cortez, J. Sánchez-Valente, J. Nagira, Catal. Today 109 (2005) 69–75.
[4] F. Rodríguez-Reinoso, Carbon 36 (3) (1998) 159–175.
[5] A.R. Lillian, Energy Fuels 7 (1993) 937–942.
[6] F.J. Derbyshire, V.H.J. de Beer, G.M.K. Abotsi, A.W. Scaroni, J.M. Solar, D.J. Skrovanek, Appl. Catal. 27 (1986) 117–131.
[7] M. Molina-Sabio, M.T. González, F. Rodríguez-Reinoso, A. Sepúlveda-Escribano, Carbon 34 (4) (1996) 505–509.
[8] S. Yamazoe, US Patent 5,672,873 (1997).
[9] L.S. Kotlyar, D.S. Montgomery, J.R. Woods, B.D. Sparks, J.A. Ripmeester, in: Proceedings of Eastern Oil Shale Symposium, 15–17, 1989, pp. 68–73.
[10] K.S.W. Sing, D.H. Everett, R.A.W. Haul, L. Moscou, R.A. Pierotti, J. Rouquerol, T. Siemieniewska, Pure Appl. Chem. 57 (4) (1985) 603–619.
[11] S.K. Ryu, H. Jin, D. Gondy, N. Pusset, P. Ehrburger, Carbon 31 (1983) 841–842.
[12] W.F. DeGroot, G.N. Richards, Carbon 27 (2) (1989) 247–252.
[13] F. Rodríguez-Reinoso, M. Molina-Sabio, M.T. González, Carbon 33 (1) (1995) 15–23.
[14] T. Wigmans, Carbon and Coal Gasification Science and Technology, Martinus Nijhoff Publishers, 1986, pp. 559–599.
[15] J. Pastor-Villegas, C.J. Durán-Valle, Carbon 40 (2002) 397–402.
[16] G. Hall, S.P. Herron, Adv. Chem. Ser. 195 (1981) 137–153.
[17] H. Fukuyama, S. Terai, Petroleum Sci. Technol. 25 (2007) 231–240.